Analysis of Common-Mode Noise on On-Chip Differential Lines through Stochastic Modeling of Parameter Variability

Dries Vande Ginste [#1], Daniël De Zutter [#2], Dirk Deschrijver [#3], Tom Dhaene [#4],
Paolo Manfredi [*5], Flavio Canavero [*6]

 # Department of Information Technology, Ghent University
Sint-Pietersnieuwstraat 41, B-9000 Gent, Belgium
[1] `Dries.VandeGinste@UGent.be`
[2] `Daniel.DeZutter@UGent.be`
[3] `Dirk.Deschrijver@UGent.be`
[4] `Tom.Dhaene@UGent.be`

* Dipartimento di Elettronica, Politecnico di Torino
Corso Duca degli Abruzzi 24, 10129 Torino, Italy
[5] `Paolo.Manfredi@polito.it`
[6] `Flavio.Canavero@polito.it`

Abstract—In this contribution a novel stochastic modeling strategy to analyze the influence of parameter variability on differential signaling over on-chip interconnects is presented. The method starts from an accurate computation of the differential line's per unit of length transmission line parameters, adopts a parameterized macromodeling scheme, and invokes the so-called stochastic Galerkin method (SGM). Parameter variability of the line itself and of the terminations are studied and compared to a traditional Monte Carlo (MC) approach, as such demonstrating excellent accuracy and efficiency of the proposed new technique. For the first time, an SGM is constructed for and applied to differential on-chip interconnects, and it is illustrated that this novel stochastic modeling strategy is very well suited to analyze common-mode noise induced by random imbalance of the line's terminations.

I. INTRODUCTION

It is nowadays a well-known fact that the electromagnetic compatibility (EMC) and signal integrity (SI) behavior of state-of-the-art interconnect structures is largely influenced by their manufacturing process. Due to production tolerances, geometrical and material parameter uncertainty appears and randomness is introduced. This is especially the case for on-chip interconnects, where increasing miniaturization only adds to the problem. Positions and widths of the traces are no longer deterministically known and also the shape of the cross-section can be influenced, e.g. by etching or electrolytic growth, leading to random trapezoidal cross-sections of the metallic interconnects, instead of rectangular ones [1]. On top of that, designers have to deal with very stringent design specifications, making it imperative to rely on efficient and accurate modeling tools, which accurately predict all high-frequency phenomena and effects induced by the substrate and conductor loss mechanisms (skin effect, slow-wave effect, etc). In recent literature the stochastic Galerkin

method (SGM) [2] has been applied to uniform transmission lines, in particular to cable harnesses [3] and interconnects on printed circuit boards [4]. The technique relies on simple numerical schemes or on heuristic models for the per unit of length (p.u.l.) parameters of the uniform multiconductor transmission lines (MTL) under consideration. These p.u.l. parameters were considered to be frequency independent. Unfortunately, the SGM, as presented in [3] and [4], cannot be immediately applied to on-chip interconnect structures, especially not in the presence of semiconductors, because the on-chip interconnects' p.u.l. parameters are strongly frequency dependent and also strongly influenced by material and geometrical parameters. Hence, simple numerical schemes or heuristic models do not suffice.

In [5], parameter variability of on-chip interconnects was studied, using a simple but robust Monte Carlo (MC) approach. It is well-known that the convergence of MC is problematic, leading to very long simulations times. For the single on-chip line in the presence of one stochastic parameter, as presented in [5], however, the MC analysis was made tractable via a macromodeling step. Unfortunately, the technique of [5] is not readily extendable to MTLs in the presence of multiple stochastic parameters.

In this contribution, a novel stochastic modeling strategy is proposed for on-chip interconnects. A three-step approach is adopted. First, the p.u.l. parameters of the MTL are accurately computed, using a two-dimensional (2-D) electromagnetic (EM) modeling tool [6], [7]. Second, the tabulated data evolving from the first step are used as input for a macromodeling procedure, yielding parameterized multivariate macromodels for the pertinent p.u.l. parameters. Thanks to the construction of these macromodels, which are closed-form expressions, in a third step, an accurate and efficient SGM can be implemented.

Whereas in [8] the general framework is explained in great detail, this contribution focusses on some important aspects concerning EMC and SI. First, and in contrast to [8], the lines' terminations are also considered as random variables (RVs). Second, differential lines are studied, and more specifically, the appearance of common-mode noise, induced by random imbalance of the terminations, is analyzed. It is demonstrated that the proposed stochastic modeling strategy leads to accurate results in an elegant and efficient way, compared to standard MC approaches.

II. MACROMODELING BASED STOCHASTIC GALERKIN METHOD FOR ON-CHIP INTERCONNECTS

The goal is to solve the Telegrapher's equations pertaining to MTLs that are influenced by a set of stochastic parameters, which can be geometrical or material parameters of the interconnect structure itself, or parameters describing the non-deterministic character of the terminations of the lines. In this section, for clarity of explanation, a single line with a single stochastic parameter is considered; more general expressions can be found in [8]. In Section III, examples with up to four parameters will be discussed. The pertinent Telegrapher's equations for this simplified case are

$$\frac{d}{dz}V(z,s,\beta) = -Z(s,\beta)\,I(z,s,\beta), \qquad (1)$$

$$\frac{d}{dz}I(z,s,\beta) = -Y(s,\beta)\,V(z,s,\beta), \qquad (2)$$

where $V(z,s,\beta)$ and $I(z,s,\beta)$ are the voltage and the current along the line and these are functions of the distance z along the line, the complex frequency $s = j2\pi f$ and of the stochastic parameter β. The p.u.l. impedance $Z(s,\beta)$ and admittance $Y(s,\beta)$ are also function of s and β.

In a first step, these p.u.l. parameters need to be very accurately computed. Thereto, a 2-D EM modeling tool [6], [7] is used. This solver assumes a quasi-TM behavior of the fields, which is a valid assumption for on-chip interconnects, given their electrically small cross-sections. A careful definition of the circuit current in the presence of the semiconductors leads to a consistent formulation of the complex inductance and complex capacitance problems, which are cast as boundary integral equations (BIEs). This is made possible thanks to the introduction of a discretized version of the Dirichlet-to-Neumann boundary operator. Solving the two BIEs for a set of samples (s,β) yields tabulated data for $Z(s,\beta)$ and $Y(s,\beta)$. The data samples so obtained are very accurate: all high-frequency phenomena are very precisely captured, as well as all loss mechanisms. Because of the BIE-approach, the technique is also rather efficient, as the skin-effect is accurately modeled without needing a very fine volume discretization.

Second, multivariate parameterized macromodels [9] are constructed starting from this tabulated data. For V fixed values of the stochastic parameter β_v, $v = 1, \ldots, V$, univariate macromodels $Z^{\mathrm{umm}}(s,\beta_v)$ and $Y^{\mathrm{umm}}(s,\beta_v)$ for the p.u.l. parameters are obtained via a standard Vector Fitting (VF) routine [10]–[12] in combination with adaptive frequency sampling [13]. These univariate macromodels, which are rational

functions of frequency, are then strung together by means of barycentric interpolation [14]:

$$Z^{\mathrm{mm}}(s,\beta) = \left(\sum_{v=1}^{V} \frac{w_v}{\beta - \beta_v} Z^{\mathrm{umm}}(s,\beta_v) \right) \Big/ \left(\sum_{v=1}^{V} \frac{w_v}{\beta - \beta_v} \right), \qquad (3)$$

$$Y^{\mathrm{mm}}(s,\beta) = \left(\sum_{v=1}^{V} \frac{w_v}{\beta - \beta_v} Y^{\mathrm{umm}}(s,\beta_v) \right) \Big/ \left(\sum_{v=1}^{V} \frac{w_v}{\beta - \beta_v} \right), \qquad (4)$$

where the numbers w_v, $v = 1, \ldots, V$, indicate the pertinent barycentric weights.

Third, the SGM is invoked. To this end, a polynomial chaos (PC) expansion of the unknown voltage and current along the line and of the known p.u.l. parameters is put forward, as follows:

$$V(z,s,\beta) = \sum_{k=0}^{K} V_k(z,s)\,\phi_k(\beta), \qquad (5)$$

$$I(z,s,\beta) = \sum_{k=0}^{K} I_k(z,s)\,\phi_k(\beta), \qquad (6)$$

$$Z^{\mathrm{mm}}(s,\beta) = \sum_{k=0}^{K} Z_k(s)\,\phi_k(\beta), \qquad (7)$$

$$Y^{\mathrm{mm}}(s,\beta) = \sum_{k=0}^{K} Y_k(s)\,\phi_k(\beta). \qquad (8)$$

In the above equations, the functions $\phi_k(\beta)$, $k = 0, \ldots, K$, are a set of $K+1$ orthogonal polynomials pertaining to the Wiener-Askey scheme [15], satisfying

$$<\phi_k(\beta), \phi_m(\beta)> = <\phi_m(\beta), \phi_m(\beta)> \,\delta_{km}, \qquad (9)$$

with δ_{km} the Kronecker delta and where the Hilbert space of the variable β is equipped with the inner product

$$<\phi_k(\beta), \phi_m(\beta)> = \int_a^b \phi_k(\beta)\,\phi_m(\beta)\,W_\beta(\beta)\,d\beta. \qquad (10)$$

In (10), the weighting function $W_\beta(\beta)$ denotes the probability distribution of β. For example, in the case that β is uniformly distributed in the interval $[a,b]$, the weighting function $W_\beta(\beta)$ is a constant, and the polynomials $\phi_k(\beta)$ are Legendre polynomials. For a normal distributed RV β, $W_\beta(\beta)$ is a Gaussian weighting function, the interval $[a,b] =]-\infty, \infty[$ extends over the complete real axis, and Hermite polynomials have to be adopted. From this scheme, and using the closed-form expressions (3) and (4), the expansion coefficients $Z_k(s)$ and $Y_k(s)$, $k = 0, \ldots, K$, of the p.u.l. parameters can be accurately and efficiently obtained, as follows:

$$Z_k(s) = <Z^{\mathrm{mm}}(s,\beta), \phi_k(\beta)> \,/\, <\phi_k(\beta), \phi_k(\beta)>, \quad (11)$$

$$Y_k(s) = <Y^{\mathrm{mm}}(s,\beta), \phi_k(\beta)> \,/\, <\phi_k(\beta), \phi_k(\beta)>. \quad (12)$$

To solve now for the $2(K+1)$ unknown expansion coefficients $V_k(z,s)$ and $I_k(z,s)$, $k = 0, \ldots, K$, the expansions (5), (6), (7) and (8) are substituted back into the Telegrapher's

145

equations (1) and (2), which are then subject to a Galerkin weighting procedure, meaning that the equations are weighted with the same set of test functions $\phi_m(\beta)$, $m = 0, \ldots, K$, using the inner product (10). This leads to a set of $2(K+1)$ coupled equations in the unknown expansion coefficients, as follows:

$$\forall m = 0, \ldots, K :$$

$$\frac{d}{dz}V_m(z,s) = -\sum_{k=0}^{K}\sum_{l=0}^{K}\alpha_{klm}Z_k(s)I_l(z,s), \quad (13)$$

$$\frac{d}{dz}I_m(z,s) = -\sum_{k=0}^{K}\sum_{l=0}^{K}\alpha_{klm}Y_k(s)V_l(z,s), \quad (14)$$

with

$$\alpha_{klm} = <\phi_k(\beta)\phi_l(\beta), \phi_m(\beta)> / <\phi_m(\beta), \phi_m(\beta)> . \quad (15)$$

Equations (13) and (14) correspond to a matrix ordinary differential equation (ODE). Compared to the original equations (1) and (2), the dimensionality is increased, but the dependency on the stochastic parameter(s) is removed. The ODE can be solved upon the knowledge of $2(K+1)$ boundary conditions (BCs). Therefore, consider a finite length $\mathcal{L}$ of the line, which is now terminated by means of Thévenin generators at both its ends. These Thévenin generators consist of a voltage source $E_N(s,\beta)$ and an impedance $Z_N(s,\beta)$ at the near end ($z = 0$) and of a voltage source $E_F(s,\beta)$ and an impedance $Z_F(s,\beta)$ at the far end ($z = \mathcal{L}$). Then, the two port equations at the terminations of the lines are

$$V_N(s,\beta) = E_N(s,\beta) - Z_N(s,\beta)\,I_N(s,\beta), \quad (16)$$

$$V_F(s,\beta) = E_F(s,\beta) + Z_F(s,\beta)\,I_F(s,\beta), \quad (17)$$

where $V_N(s,\beta) \equiv V(z = 0,s,\beta)$, $V_F(s,\beta) \equiv V(z = \mathcal{L},s,\beta)$, $I_N(s,\beta) \equiv I(z = 0,s,\beta)$ and $I_F(s,\beta) \equiv I(z = \mathcal{L},s,\beta)$ denote the port voltages and currents. It is observed that also the Thévenin generators can depend on one or more stochastic parameters. The two equations (16) and (17) are now also subject to the SGM procedure, leading to the proper set of $2(K+1)$ BCs:

$$\forall m = 0, \ldots, K :$$

$$V_{N,m}(s) = E_{N,m}(s) - \sum_{k=0}^{K}\sum_{l=0}^{K}\alpha_{klm}Z_{N,k}(s)I_{N,l}(s), \quad (18)$$

$$V_{F,m}(s) = E_{F,m}(s) + \sum_{k=0}^{K}\sum_{l=0}^{K}\alpha_{klm}Z_{F,k}(s)I_{F,l}(s). \quad (19)$$

These BCs are used to solve (13) and (14). Once the coefficients $V_k(s)$ and $I_k(s)$, $k = 0, \ldots, K$, are known, they are substituted back into (5) and (6), yielding the final current and voltage along the line as a function of frequency, and as a function of the stochastic parameter(s) β. For this latter, only a pertinent probability distribution was considered. The stochastic moments or probability distribution of the voltage and current can now be calculated using standard analytical or numerical techniques [16].

III. Variability Analysis of On-Chip Differential Lines

A. Geometry

As an example, we consider a pair of coupled inverted embedded microstrip (IEM) lines, of which the cross-section is shown in Fig. 1. This structure comprises a semiconductor substrate, i.e. 30 μm Silicon with a relative permittivity of 11.7 and a conductivity of 10 S/m, and a 11.4 μm thick SiO$_2$ insulator with a relative permittivity of 3.9 and a loss tangent of 0.001. The ground plane is placed on top of the layered structure and it is made out of 3 μm thick Aluminum with a conductivity of $3.77 \cdot 10^7$ S/m. The signal conductors are found at a height of 6.4 μm above the semiconductor-insulator interface. They are made out of 2 μm thick Aluminum. Whereas the top sides of these lines are fixed to 2 μm, the base β of their cross-sections is considered to be random. The random trapezoidal shape, so obtained, is induced by the manufacturing process (etching or electrolytic growth). In the remainder of this contribution it is assumed that β is a Gaussian RV with a mean value $\mu_\beta = 2$ μm and a normalized standard deviation $\sigma_\beta = 10\%$. A second stochastic parameter is introduced, i.e. the gap ζ between the lines. The RV ζ is also normally distributed, with mean value $\mu_\zeta = 3$ μm and a normalized standard deviation $\sigma_\zeta = 8\%$. Obviously, the accuracy of these process-dependent input parameters determines the accuracy of the final result. With this differential pair of IEM lines the source-line-load configuration of Fig. 2 is now constructed. The lines are given a length of $\mathcal{L} = 1$ mm. At the near ends, low-impedance voltage sources, with an internal impedance of 1 Ω, are connected. To obtain differential steering, the voltage source on the first line has an amplitude of half a volt ($E_N^{(1)} = 500$ mV), whereas the other produces minus half a volt ($E_N^{(2)} = -500$ mV). At the far ends, the lines are terminated by a capacitive load $Z_L^{(i)} = 1/(s\,C_i)$, $i = 1, 2$.
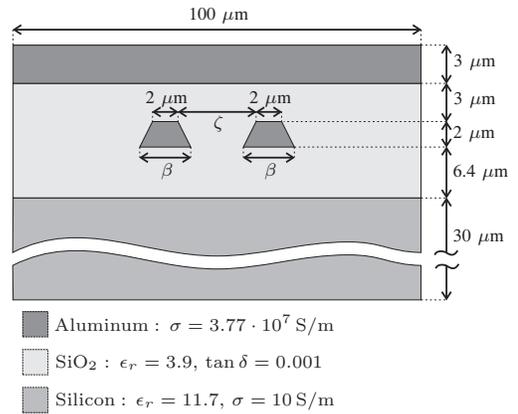

Fig. 1: Cross-section AA' (see Fig. 2) of the differential IEM lines (not on scale).

We will conduct two numerical experiments and observe the voltages at the loads. More specifically, we are interested
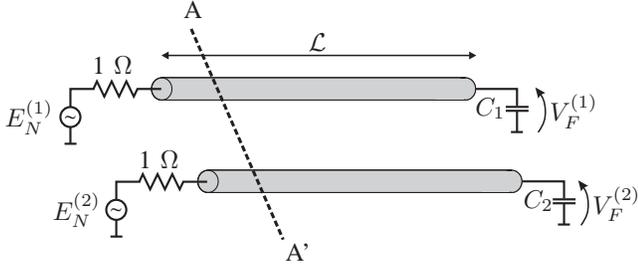
Fig. 2: Source-line-load configuration. The cross-section AA'
is depicted in Fig. 1.

in the differential signal voltage V_d and the common signal voltage V_c, which are defined as [17]:

$$V_d = V_F^{(1)} - V_F^{(2)}, \tag{20}$$

$$V_c = \frac{V_F^{(1)} + V_F^{(2)}}{2}. \tag{21}$$

B. Balanced lines

In a first experiment we consider the capacitive loads to be deterministic and equal, i.e. $C_1 = C_2 = 1$ pF. A variability analysis is performed, using the novel modeling strategy outlined in Section II and an MC run with 50000 (β, ζ)-samples. A Bode plot of the magnitude of the differential voltage (20) is shown in Fig. 3(a) for a frequency range up to 100 GHz and a magnification of the resonance around 8 GHz is shown in Fig. 3(b). Thanks to the symmetric configuration with balanced loads and the differential excitation, the common-mode voltage (21) is of course zero, and hence, not displayed. In Fig. 3, the full black lines indicate the mean $\mu_{|V_d|}$, and the dashed lines show the $\pm 3\sigma_{|V_d|}$ deviations from this mean, all computed using the novel approach. The gray lines on the figures correspond to 100 samples of the MC run; the circles ($\circ$) and squares ($\square$) indicate the mean and the $\pm 3\sigma$-deviations, resp., computed using the 50000 samples of the MC run. (For clarity, the circles and squares are not shown on Fig. 3(a).) From Fig. 3 an excellent agreement between the MC analysis and the novel technique is observed. Comparison of CPU times between the two techniques indicates that the novel SGM is more than 200 times faster than the MC run. Apart from stochastic moments, complete stochastic functions can be computed as well. In Fig. 4 the probability density function (PDF) and the cumulative distribution function (CDF) of the differential voltage's magnitude at 8 GHz are presented. Excellent agreement is again observed.

C. Common-mode noise induced by random loads

In this second experiment, the capacitive loads are now also considered to be prone to manufacturing tolerances, and hence, in addition to the trapezoids' base length β and the gap ζ, the capacitors are modeled as stochastic parameters. Specifically, we consider C_1 and C_2 to be mutually independent RVs that are both uniformly distributed within the interval $[0.9, 1.1]$ pF. Of course, an imbalance can occur now, so we analyze both the differential voltage and the common-mode voltage. In
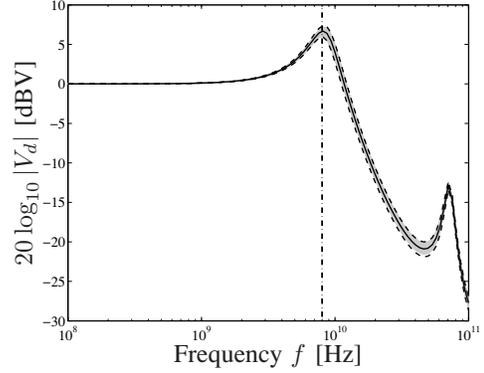
(a) $|V_d|$ as a function of frequency
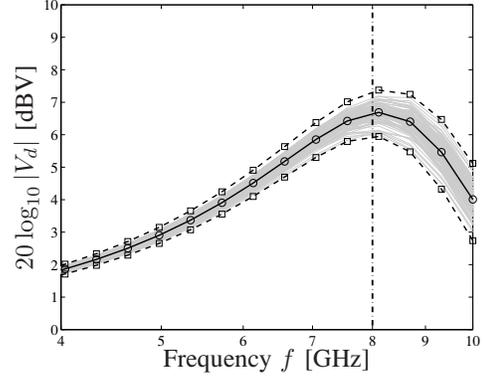
(b) Detail of Fig. 3(a) around 8 GHz, clearly illustrating the effect of the stochastic parameters

Fig. 3: Bode plot of the magnitude of the differential voltage V_d for the balanced differential IEM lines. Full black line: mean $\mu_{|V_d|}$ computed using the novel technique; Dashed black line: $\pm 3\sigma_{|V_d|}$-variations computed using the novel technique; Gray lines: 100 samples from the MC run; Circles ($\circ$): mean $\mu_{|V_d|}$ computed using MC technique; Squares ($\square$): $\pm 3\sigma_{|V_d|}$-variations computed using MC technique.
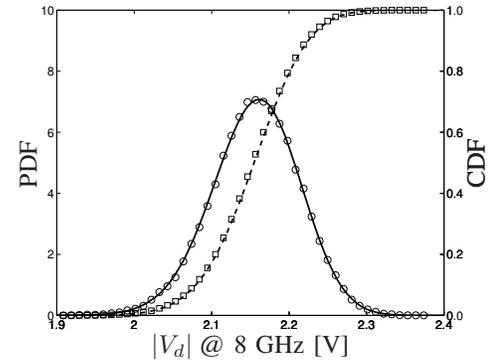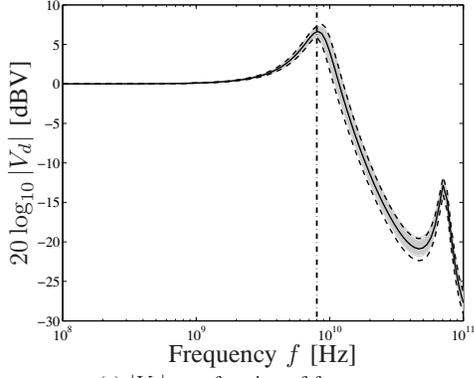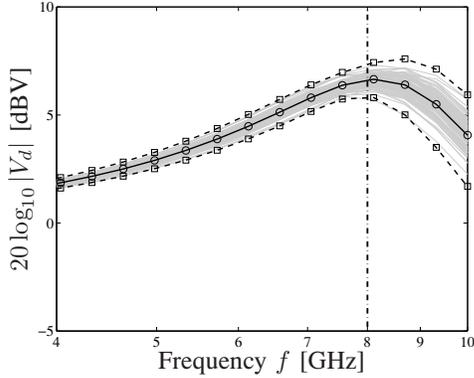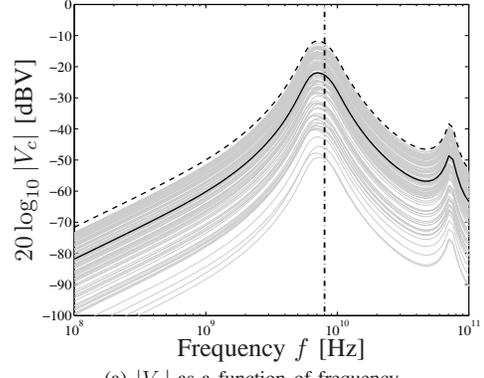

Fig. 4: PDF and CDF of the magnitude of the differential voltage V_d at 8 GHz for the balanced differential IEM lines. Full black line: PDF computed using the novel technique; Dashed black line: CDF computed using the novel technique; Circles ($\circ$): PDF computed using MC technique; Squares ($\square$): CDF computed using MC technique.
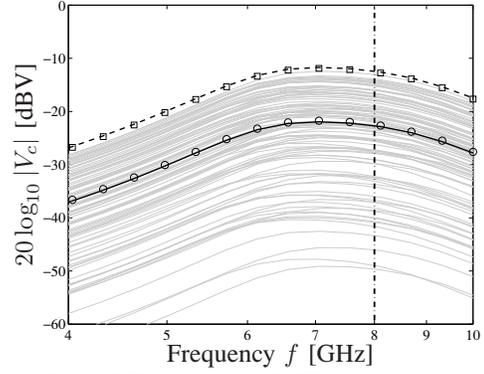
147

(a) $|V_d|$ as a function of frequency

(b) Detail of Fig. 5(a) around 8 GHz, clearly illustrating the effect of the stochastic parameters

Fig. 5: Bode plot of the magnitude of the differential voltage V_d for the unbalanced differential IEM lines. Full black line: mean $\mu_{|V_d|}$ computed using the novel technique; Dashed black line: $\pm 3\sigma_{|V_d|}$-variations computed using the novel technique; Gray lines: 100 samples from the MC run; Circles ($\circ$): mean $\mu_{|V_d|}$ computed using MC technique; Squares ($\square$): $\pm 3\sigma_{|V_d|}$-variations computed using MC technique.

(a) $|V_c|$ as a function of frequency

(b) Detail of Fig. 6(a) around 8 GHz, clearly illustrating the effect of the stochastic parameters

Fig. 6: Bode plot of the magnitude of the common-mode voltage V_c for the unbalanced differential IEM lines. Full black line: mean $\mu_{|V_c|}$ computed using the novel technique; Dashed black line: $+3\sigma_{|V_c|}$-variation computed using the novel technique; Gray lines: 100 samples from the MC run; Circles ($\circ$): $\mu_{|V_c|}$ computed using MC technique; Squares ($\square$): $+3\sigma_{|V_c|}$-variation computed using MC technique.
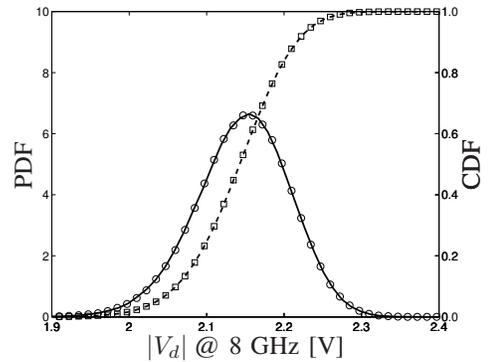

Fig. 7: PDF and CDF of the magnitude of the differential voltage V_d at 8 GHz for the unbalanced differential IEM lines. Full black line: PDF computed using the novel technique; Dashed black line: CDF computed using the novel technique; Circles ($\circ$): PDF computed using MC technique; Squares ($\square$): CDF computed using MC technique.

Figs. 5(a) and 6(a) the magnitude of both quantities are shown, using the novel SGM approach and an MC run with 50000 (β, ζ, C_1, C_2)-samples, for a frequency range up to 100 GHz. In Figs. 5(b) and 6(b) a magnification of the differential voltage's resonance around 8 GHz is shown. As before, the full black lines indicate the mean values $\mu_{|V_d|}$ and $\mu_{|V_c|}$, and the dashed lines show the $\pm 3\sigma_{|V_d|}$ and $+3\sigma_{|V_c|}$ deviations from these mean values, all computed using the novel approach. The gray lines on the figures correspond to 100 samples of the MC run; the circles ($\circ$) and squares ($\square$) indicate the mean values and the 3σ-deviations, resp., computed using the 50000 samples of the MC run. For this unbalanced setup, $3\sigma_{|V_c|} > \mu_{|V_c|}$. Hence, the $-3\sigma_{|V_c|}$-deviations are no longer shown. From Figs. 5 and 6, an excellent agreement between the MC analysis and the novel technique is observed. It is also noticed that an important common-mode noise contribution can occur, especially around 7 GHz where a peak appears. In Figs. 7 and 8, the PDF and the CDF of the (desired) differential voltage and the common-mode voltage (noise) at 8 GHz are
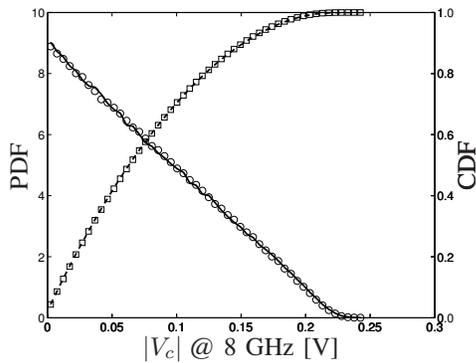
Fig. 8: PDF and CDF of the magnitude of the common-mode voltage V_c at 8 GHz for the unbalanced differential IEM lines. Full black line: PDF computed using the novel technique; Dashed black line: CDF computed using the novel technique; Circles (○): PDF computed using MC technique; Squares (□): CDF computed using MC technique.

shown, as such allowing a comparison with the balanced case of Fig. 4. In contrast to the differential voltage, which is not much affected, the PDF of the common-mode voltage is very skew. This can be explained as follows: given the two uniform distributions of the loads, in many instances the lines will be rather balanced, yielding a high probability of a low common-mode noise voltage. However, a significant noise contribution of more than 200 mV is also possible. Because of the skewness of the PDF, a thorough validation of the technique is obtained. Typically, such skew PDFs can no longer be described by only low order stochastic moments, and are harder to model. It is interesting to mention that the above figures provide valuable information for interconnect designers, allowing to rapidly assess the signal integrity behavior of the interconnect. For example, Figs. 7 and 8 lead to the conclusion that, at the loads, a maximum common-mode noise contribution of about 10% w.r.t. the desired differential signal can be expected.

In all of the above examples, the material parameters were considered to be constant. Of course, frequency-dependent material parameters are easily included, as the proposed technique is a frequency-domain method. For completeness, we also mention that, given this frequency-domain approach, nonlinear terminations cannot be included in a straightforward way.

IV. CONCLUSION

In this contribution a novel SGM was presented to analyze parameter variability of on-chip differential lines. The influence of multiple stochastic parameters was studied, such as shape of the cross-section, gap between the lines, and loads of the lines. The randomness of these parameters is induced by the manufacturing process. The new SGM for these on-chip lines was made possible thanks to very accurate 2-D EM modeling *and* parameterized macromodeling of the pertinent p.u.l. transmission line parameters. Upon comparison with a standard MC technique, the accuracy and efficiency of the novel modeling strategy was validated. Illustrative examples show that the technique allows analyzing signal integrity aspects of on-chip differential lines, and in particular, it allows to rapidly assess the maximum common-mode noise contribution that can be expected at the terminations.

REFERENCES

[1] F.-L. Lin and R.-B. Wu, "Analysis of coplanar-waveguide discontinuities with finite-metallization thickness and nonrectangular edge profile," *IEEE Trans. Microw. Theory Tech.*, vol. 45, no. 12, pp. 2131–2137, Dec. 1997.

[2] D. Xiu, "Fast numerical methods for stochastic computations: A review," *Communications in Computational Physics*, vol. 5, no. 2-4, pp. 242–272, Feb. 2009.

[3] I. S. Stievano, P. Manfredi, and F. G. Canavero, "Stochastic analysis of multiconductor cables and interconnects," *IEEE Trans. Electromagn. Compat.*, vol. 53, no. 2, pp. 501–507, May 2011.

[4] ——, "Parameters variability effects on multiconductor interconnects via hermite polynomial chaos," *IEEE Trans. on Components, Packaging and Manufacturing Technology*, vol. 1, no. 8, pp. 1234–1239, Aug. 2011.

[5] D. Vande Ginste, D. De Zutter, D. Deschrijver, T. Dhaene, and F. Canavero, "Macromodeling based variability analysis of an inverted embedded microstrip line," in *Proc. of the 20th IEEE Int. Conf. on Electrical Performance of Electronic Packaging and Systems (EPEPS)*, San Jose, CA, USA, 23 - 26 Oct. 2011, pp. 153–156.

[6] T. Demeester and D. De Zutter, "Quasi-TM transmission line parameters of coupled lossy lines based on the Dirichlet to Neumann boundary operator," *IEEE Trans. Microw. Theory Tech.*, vol. 56, no. 7, pp. 1649–1660, Jul. 2008.

[7] T. Demeester, D. Vande Ginste, and D. De Zutter, "Accurate study of the electromagnetic and circuit behavior of finite conducting wedges and interconnects with arbitrary cross-sections," in *Proc. of 19th IEEE Int. Conf. on Electrical Performance of Electronic Packaging and Systems (EPEPS)*, Austin, TX, USA, 24 - 27 Oct. 2010, pp. 133–136.

[8] D. Vande Ginste, D. De Zutter, D. Deschrijver, T. Dhaene, P. Manfredi, and F. Canavero, "Stochastic modeling based variability analysis of on-chip interconnects," *Accepted for IEEE Transactions on Components, Packaging and Manufacturing Technology*, Mar. 2012.

[9] D. Deschrijver and T. Dhaene, "Stability and passivity enforcement of parametric macromodels in time and frequency domain," *IEEE Trans. Microw. Theory Tech.*, vol. 56, no. 11, pp. 2435–2441, Nov. 2008.

[10] B. Gustavsen and A. Semlyen, "Rational approximation of frequency domain responses by vector fitting," *IEEE Trans. Power Del.*, vol. 14, no. 3, pp. 1052–1061, Jul. 1999.

[11] B. Gustavsen, "Improving the pole relocating properties of vector fitting," *IEEE Trans. Power Del.*, vol. 21, no. 3, pp. 1587–1592, Jul. 2006.

[12] D. Deschrijver, M. Mrozowski, T. Dhaene, and D. De Zutter, "Macromodeling of multiport systems using a fast implementation of the vector fitting method," *IEEE Microwave and Wireless Components Letters*, vol. 18, no. 6, pp. 383–385, Jun. 2008.

[13] G. Antonini, D. Deschrijver, and T. Dhaene, "Broadband rational macromodeling based on the adaptive frequency sampling algorithm and the partial element equivalent circuit method," *IEEE Trans. Electromagn. Compat.*, vol. 50, no. 1, pp. 128–137, Feb. 2008.

[14] J. P. Berrut and L. N. Trefethen, "Barycentric Lagrange interpolation," *SIAM Review*, vol. 46, no. 3, pp. 501–517, Sep. 2004.

[15] D. Xiu and G. E. Karniadakis, "The Wiener-Askey polynomial chaos for stochastic differential equations," *SIAM J. Sci. Comput.*, vol. 24, no. 2, pp. 619–644, 2002.

[16] A. Papoulis, *Probability, Random Variables, and Stochastic Processes*, 3rd ed. McGraw-Hill, 1991.

[17] E. Bogatin, *Signal and Power Integrity — Simplified*, 2nd ed. Prentice Hall, 2009.